THE JOURNAL OF PHYSICAL CHEMISTRY C
A JOURNAL OF THE AMERICAN CHEMICAL SOCIETY

pubs.acs.org/JPCC

Article

Local Wear of Catechol-Containing Diblock Copolymer Layers: Wear Volume, Stick–Slip, and Nanomechanical Changes

Published as part of The Journal of Physical Chemistry virtual special issue "Marie-Paule Pileni Festschrift".

Illia Dobryden,* Medeina Steponavičiūtė, Daniel Hedman, Vaidas Klimkevičius, Ričardas Makuška, Andra Dėdinaitė, Xiaoyan Liu, Robert W. Corkery, and Per Martin Claesson*

Cite This: *J. Phys. Chem. C* 2021, 125, 21277–21292

Read Online

ACCESS | Metrics & More | Article Recommendations | Supporting Information

ABSTRACT: Polymers containing catechol groups have gained a large interest, as they mimic an essential feature of mussel adhesive proteins that allow strong binding to a large variety of surfaces under water. This feature has made this class of polymers interesting for surface modification purposes, as layer functionalities can be introduced by a simple adsorption process, where the catechol groups should provide a strong anchoring to the surface. In this work, we utilize an AFM-based method to evaluate the wear resistance of such polymer layers in water and compare it with that offered by electrostatically driven adsorption. We pay particular attention to two block copolymer systems where the anchoring group in one case is an uncharged catechol-containing block and in the other case a positively charged and catechol-containing block. The wear resistance is evaluated in terms of wear volume, and here, we compare with data for similar copolymers with statistical distribution of the catechol groups. Monitoring of nanomechanical properties provides an alternative way of illustrating the effect of wear, and we use modeling to show that the stiffness, as probed by an AFM tip, of the soft layer residing on a hard substrate increases as the thickness of the layer decreases. The stick–slip characteristics are also evaluated.

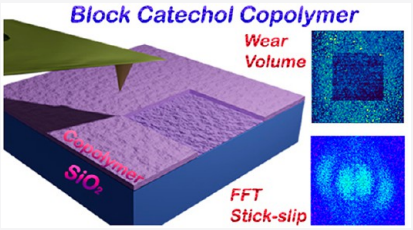

INTRODUCTION

The pioneering work of Waite and co-workers[1−3] provided an understanding of the role of the structure and composition of the cationic adhesion proteins used by the mussel *Mytilus edulis* to strongly bind to surfaces under water. They recognized the importance of a repeating decapeptide containing the unusual amino acid 3,4-dihyroxyphenylalanine (DOPA) for the underwater adhesion, and the foot protein with the highest DOPA content was found to predominate at the adhesion point to the solid substrate.[3] Remarkably, strong underwater adhesion is found to nearly all types of surfaces, even Teflon, even though the adhesion strength depends on the nature of the solid.[3] The key feature of DOPA is the presence of two OH groups separated by a single carbon−carbon bond, as also found in catechol. The strong underwater adhesion offered by DOPA and catechol has inspired significant efforts in the preparation of bioinspired synthetic adhesion polymers[4−11] and functional materials.[12] There are several excellent reviews covering different aspects of these developments.[13−19]

The binding modes of mussel adhesive proteins, DOPA, and catechol to different surfaces have been investigated both experimentally and theoretically. The picture that is emerging is quite complex. Some early studies reported the importance of the complex formation ability of catechol and DOPA. For instance, complex formation between aluminum and catechol was pointed out as being of importance for binding of catechol to aluminum oxides,[20] and complex formation between Fe(III) and DOPA was highlighted as an important physical cross-linking mechanism.[21] This was later emphasized in studies showing increased corrosion protection of carbon steel with time when thin films containing mussel adhesive proteins were utilized as a protecting agent.[22−24] Surface force measurements have demonstrated a stronger binding to titanium dioxide than to mica.[25] In both cases, bidentate hydrogen bonds between DOPA and the surface were regarded as being of paramount importance, and the difference in adhesion to the two surfaces was suggested to be due to the larger covalent character of the hydrogen bonds between DOPA and titanium dioxide. Consequently, oxidation of DOPA to dopaquinone reduces the adhesion force to titanium dioxide surfaces, as demonstrated by contact mechanics adhesion tests using DOPA-containing hydrogels.[26] Bidentate hydrogen bonds between DOPA and silica have also been suggested as being of primary importance for the adhesion strength.[27] It has also been suggested that DOPA can form covalent bonds with primary amines and

Received: August 3, 2021
Published: September 21, 2021

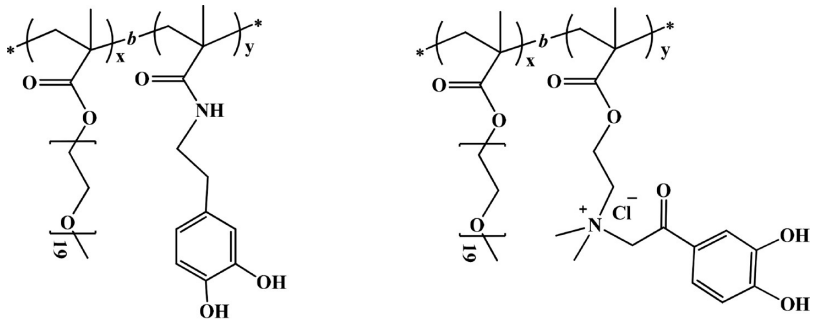

Figure 1. Structures of the diblock copolymers. The chemical names and the abbreviations we use in this paper are p(PEO_{19}MEMA)-*b*-p(DOPMA), PEO-*b*-catechol, and p(PEO_{19}MEMA)-*b*-p(MEDAPDAC), PEO-*b*-cationic-catechol.

Table 1. Chemical Name, Abbreviation, and Key Properties of the Copolymers

copolymer		properties			
chemical name	abbreviation	composition PEO_{19}MEMA (mol %)	Mn (kDa)	dispersity, $Đ$	degree of polymerization, DP
p(PEO_{19}MEMA)-*b*-p(DOPMA)	PEO-*b*-catechol	46	52.7	1.37	94
p(PEO_{19}MEMA)-*b*-p(MEDAPDAC)	PEO-*b*-cationic-catechol	51	54.8	1.23	98
p(PEO_{19}MEMA-*s*-METAC)	PEO-*s*-cationic	46	62.5	1.18	103
p(PEO_{19}MEMA-*s*-DOPMA)	PEO-*s*-catechol	56	55.4	1.19	88
p(PEO_{19}MEMA-*s*-MEDAPDAC)	PEO-*s*-cationic-catechol	46	61.9	1.13	99

thiols,[12] that electrostatic forces contribute to the adhesion between negatively charged surfaces and cationic mussel adhesive proteins,[28] and that hydrophobic interactions contribute to the adhesion to non-polar surfaces.[29] Vibrational sum frequency spectroscopy studies have suggested that $\pi-\pi$ stacking contributes to the adhesion to surfaces such as polystyrene.[30]

Clearly, many different adhesion modes are available to the mussel adhesive proteins in particular but also to the DOPA and catechol groups. Further understanding of the adhesion mechanisms can be obtained by modeling experiments. A density functional theory study of catechol binding to silica showed that three to four hydrogen bonds could be formed between a silica surface and the catechol group (the catechol group can act as a donor in two hydrogen bonds and also as an acceptor in hydrogen bonds where surface silanol groups act as donors).[31] Thus, the hydroxyl groups and not the aromatic ring dominated the binding energy of catechol. It was found that the binding of catechol to silica was non-covalent but with a higher binding energy than that of water to silica with a binding energy difference of up to 2 kcal/mol. Thus, direct catechol−surface bonds were formed and water was displaced from the surface by the catechol moiety. Dispersion forces made the binding energy of catechol to silica even more favorable when compared to that of water binding to silica.[31] Later, molecular dynamics simulations confirmed that catechol displaced preadsorbed water molecules at the silica surface.[32] Further theoretical studies suggested that the catechol−silica bond can be broken by a force of 0.5 nN and that the binding energy, due to hydrogen bonds and dispersive interactions, in the presence of water amounts to 23 kcal/mol.[33] A similar, but slightly larger, binding energy has also been calculated for DOPA interacting with silica.[34]

We recently introduced a novel approach to compare the binding strength of different polymer layers, which utilized an AFM-based method to locally wear the adsorbed layer using shear under different loads.[35] Similar methods have been used for studying the local wear of hard surfaces[36,37] and polymer coatings[38] on the nanoscale, and the relation between stick−slip motion and abrasive wear has been highlighted.[39,40] We note that evaluation of partial wear of nanometer thin layers is particularly challenging, since the wear volume by necessity is small. An alternative is to utilize changes in local nanomechanical properties of the adsorbed layer that occur due to wear. Such properties can be measured with nanometer resolution with AFM[41] and include surface stiffness, elastic modulus, deformation, and tip−sample adhesion. Recently, Pileni and co-workers utilized such measurements for elucidating the importance of mechanical properties of self-assembled suprastructures for their localization and organization after uptake in cancer cells.[42,43]

In this work, we utilize an AFM-based technique to compare the local wear resistance of two diblock copolymers having the same buoy block but different anchoring groups, one being based on catechol groups and the other one containing both catechol and cationic functionalities. The method is based on measuring the topography and nanomechanical properties of the worn and surrounding pristine surface area after wear measurements with a hard AFM tip. We compare with previously investigated statistical copolymers[35] and extend the analysis to include the wear volume for all of these systems. It should be noted that the outcome of the experiment depends on both polymer−surface interactions and tip−polymer interactions. Since all polymers expose PEO side chains toward the solution side, the latter interaction can be expected to be rather similar for the different polymers, as also suggested by similar tip−sample adhesion values. We also present modeling results that rationalize the use of surface stiffness measurements to distinguish wear of thin soft layers on hard substrates. The stick−slip characteristics are also evaluated using a fast Fourier transformation of lateral force images captured as the tip slides across the surface.

https://doi.org/10.1021/acs.jpcc.1c06859
J. Phys. Chem. C 2021, 125, 21277−21292

MATERIALS AND METHODS

Materials. The diblock copolymers used consist of one uncharged block of poly(ethylene glycol) methyl ether methacrylate (molecular weight 950 Da, $PEO_{19}MEMA$) and one block that contains either uncharged catechol segments or positively charged catechol segments. These blocks provide strong anchoring to silica surfaces. The structure of the copolymers is provided in Figure 1. The details of the synthesis and characterization of the diblock copolymers are provided in the Supporting Information. Briefly, their composition was assessed by ^{1}H NMR spectroscopy, and the number-average molecular weight M_n and dispersity $Đ$ of the copolymers were determined by size exclusion chromatography, SEC, with triple detection. These parameters are reported in Table 1. As we compare the wear volume determined for the diblock copolymers with the corresponding similar statistical copolymers, we also include the properties of the statistical copolymers[34] (Table 1).

All solutions were made using Milli-Q water with a resistivity of 18.2 MΩ m to give a polymer concentration of 100 ppm by weight. All solutions were adjusted to pH 4, as monitored by using MQuant (Merck) pH-indicator strips (pH 2.0−9.0).

Methods. *Atomic Force Microscopy.* Wear and mechanical measurements were carried out using a JPK NanoWizard 3 Atomic Force Microscope (JPK Instruments AG, Berlin, Germany). To minimize possible tip damage, measurements were performed using diamond-like-carbon-coated probes (All-In-One-DLC, Budget Sensors). The measured normal spring constant was 7.0−7.1 N/m, and the nominal tip end radius was 10 nm. The torsional spring constant, k_t, was estimated from the known tip shape, the cantilever material properties, and the measured normal spring constant to be about 7×10^{-8} N·m/rad, following the procedure suggested by Alvarez-Asencio et al.[44] Polymer layers were formed by adsorption on cleaned silicon substrates of 22×22 mm^2 surface area for 10 min inside an AFM liquid cell using a polymer concentration of 100 ppm. This waiting time was judged sufficient based on the QCM-D data shown in the Supporting Information, where limited changes in dissipation and frequency were observed after 10 min. Next, the solution in the cell was replaced several times with Milli-Q water adjusted to pH 4 to remove all polymers that remained in the bulk solution and thus prevent self-healing of the layer by adsorption from solution when worn by the sliding AFM tip.

Wear measurements were carried out in contact mode using a tip sliding speed of around 4.5 μm/s. In one set of experiments, different loads were applied at different parts of the surface using one wear cycle. In another set of experiments, the same area was worn three times at a constant load. The worn area was in all cases about 1×1 μm^2. During the wear measurements, the lateral force (measured in mV) was monitored and lateral force images were obtained. These images provide information on stick−slip phenomena, and characteristic stick−slip lengths (if present) will be evident after 2D fast Fourier transformation (FFT) of these images. The 2D Fourier spectra of the AFM lateral force images were generated with the built-in FFT java script in ImageJ (version 1.53j). ImageJ employs a fast Hartley transform algorithm as an intermediate in generating the 2D FFT spectrum. The corresponding 1D FFT data were obtained by radial integration, using an integration angle of 25° to maximize the signal-to-noise ratio. Peaks in these spectra were fitted using Gaussian functions with three parameters: peak position, height, and width. The characteristic stick−slip length is obtained as the inverse of the peak position in k-space. The same approach[39] as well as 1D Fourier analysis of stick−slip patterns have recently been reported for other surfaces,[45,46] and in one case, it has even been correlated with bacterial adhesion.[47]

After the wear measurements, an area of about 2×2 μm^2 was imaged in quantitative imaging (QI) mode at a set point force of 25 nN. In these images, the worn 1×1 μm^2 area is located at the center. Thus, we can directly compare the topography and nanomechanical properties of the adsorbed layer in the worn and pristine area, and thus evaluate the effect of the combined action of normal and lateral forces. The nanomechanical quantities evaluated in this work require no fit to contact mechanics models and included the stiffness (i.e., the slope of the force curve at short distances between the maximum applied force and 50% of this force), the deformation (i.e., the compression of the surface at a load of 22.5 nN), and the tip−sample adhesion. We note that the deformation is given with a negative sign as the surface moves toward the tip as the layer is compressed. How these quantities are evaluated from the measured force curves has been described in numerous articles, e.g., in ref 41.

The wear volume was evaluated from the topography images obtained after the wear measurements. This was done by first setting the zero baseline area for the pristine copolymer layer around the wear mark using the JPK data processing software (v. 6.1.86). Then, the height change histogram was obtained for the chosen wear mark in negative numbers, i.e., below the zero plane of the pristine unworn layer. Knowing the exact area size and scan data points, it was possible to calculate the actual pixel size in nm^2. To obtain the volumetric wear, the height change in the histograms was multiplied by the corresponding amount of pixels and the pixel area. Thus, the wear volume is given as the decrease in thickness of the worn area multiplied by the worn surface area. The major effect is due to abrasive wear, as also seen by the material pushed to the side of the worn area, but there may also be a contribution from changes in polymer conformations that do not relax between the time of the wear measurement and the subsequent imaging of the worn area.

QCM-D. A Q-sense E4 microbalance (Biolin Scientific, Gothenburg, Sweden) was utilized for following the adsorption of the copolymers on silica sensors (QSX-303, Biolin Scientific) cleaned with 2% Hellmanex (Hellma GmbH) solution. The sensors were first immersed in the Hellmanex solution for 30 min, then rinsed with Milli-Q water, and finally dried by a gentle jet of nitrogen gas. Here we utilized sensors with silica coating (QSX-303, Biolin Scientific). The QCM-D cell itself was cleaned using 2% Deconex solution (Borer Chemie AG, Switzerland) followed by sonication for half an hour and rinsing with Milli-Q water and ethanol. All cleaning and assembly operations were carried out in a laminar flow cabinet.

The adsorption processes were followed by measurements of changes in frequency and energy dissipation of a quartz sensor. In our measurements, the dissipation change was small and we could thus evaluate the mass oscillating with the crystal (polymer and associated solvent) using the Sauerbrey model.[48] In this case, the mass, Γ_{QCM}, was evaluated using eq 1

$$\Gamma_{QCM} = -\frac{C\Delta f}{n} \tag{1}$$

where Δf is the measured frequency change, n the overtone number, and C a conversion factor equal to 0.177 mg m^{-2} Hz^{-1} for our sensors. The thickness of the adsorbed layer, t, was

https://doi.org/10.1021/acs.jpcc.1c06859
J. Phys. Chem. C 2021, 125, 21277−21292

estimated by dividing the adsorbed mass per unit area with the density of the layer, assumed to be 1 g/cm^3.

Modeling of Surface Stiffness. Finite element simulations were performed to evaluate the effect of surface thickness and tip radius on the surface stiffness measured by AFM. Both the AFM tip and the surface where explicitly modeled using a 2D rotational symmetric geometry in COMSOL Multiphysics [COMSOL Multiphysics v. 5.4, www.comsol.com, COMSOL AB, Stockholm, Sweden]. Table 2 shows the parameters defining the geometry used which is illustrated in Figure S6. For details on the boundary conditions used, see section S6 in the Supporting Information.

Table 2. Parameters Defining the Geometry Used in the Simulations[a]

parameter	value	unit
w	500	nm
t	1−128	nm
h	40	nm
R	6, 10, 14, 20	nm
θ	20	deg

[a] w is the width and t the thickness of the surface layer. While h is the height, θ is the aspect ratio, and R is the radius of the tip.

A neo-Hookean[49−51] hyperelastic material model was used to describe the soft polymer surface with Lamé parameter, μ = 5.0 MPa, bulk modulus, $\kappa = \mu/2$ = 2.5 MPa, and density ρ = 970 kg/m^3. The hard tip was modeled using a simple linear elastic material model, Young's modulus of E = 170 GPa, Poisson ratio of ν = 0.28, and density of ρ = 2329 kg/m^3. The tip remains essentially undeformed during the simulations.

Simulated force curves were obtained by time dependent simulations where the tip was given a prescribed displacement of 1 nm/s toward the surface. As the tip deforms the surface, the total displacement, x, of the tip into the surface was measured as well as the contact force, F, between the tip and the surface (in the direction perpendicular to the surface). The tip was allowed to deform the surface until a maximum von Mises stress of 19.5 MN/m^2 was obtained in the thin polymer layer. The stiffness, k, of the surface was then calculated by taking the derivate of the force curve

$$k = \frac{dF}{dx} \tag{2}$$

RESULTS AND DISCUSSION

In this part, we first briefly characterize the adsorption of the block copolymers on silica surfaces as evaluated by QCM-D measurements. The main part is then devoted to measurements of nanowear utilizing a sharp AFM tip. We qualitatively evaluate the wear by measurements of surface stiffness and quantitatively by measurements of the wear volume. Next, the reconstructed 2D FFT maps of lateral forces measured during the nanowear experiments are analyzed to provide quantification of the stick−slip length. In the last part, we rationalize the use of stiffness measurements for probing the wear of thin soft layers on hard substrates using a modeling approach.

Adsorption. Adsorption of the block copolymer layers was evaluated by following changes in frequency and dissipation as a function of time, and a set of typical data is shown in the Supporting Information (Figure S5). The data reported in Table 3 were extracted once adsorption equilibrium had been reached. The change in frequency was used to calculate the mass as described in the Methods section.

Table 3. Summary of QCM-D Data for the Copolymer Adsorption from 100 ppm Polymer Solution, pH 4, on Silica Surfaces[a]

polymer	$-\Delta f/n$ (Hz)	$\Delta D \times 10^6$	Γ_{QCM} (mg/m^2)	t (nm)
PEO-*b*-catechol	23.4 ± 0.2	1.0 ± 0.1	4.1 ± 0.1	4.1
PEO-*b*-cationic-catechol	21.3 ± 0.2	1.2 ± 0.1	3.8 ± 0.1	3.8
PEO-*s*-cationic	12.7 ± 0.2	0.6 ± 0.1	2.3 ± 0.1	2.3
PEO-*s*-catechol	21.5 ± 0.2	1.0 ± 0.1	3.8 ± 0.1	3.8
PEO-*s*-cationic-catechol	12.4 ± 0.2	0.7 ± 0.1	2.2 ± 0.1	2.2

[a] The data for the statistical copolymers are from ref 35.

For purely electrostatically driven adsorption of polyelectrolytes, the adsorbed amount at equilibrium is limited by either steric repulsion between adsorbed molecules (low charge density polyelectrolytes) or electrostatic forces that counteract further adsorption once the surface charge density of the surface has been neutralized.[52] Note, however, that the presence of the cationic groups next to the silica surface stimulates further dissociation of surface silanol groups.[53,54] Further, if there also is a non-electrostatic affinity between the polymer and the surface, then charge overcompensation may occur.[55] The two statistic cationic copolymers PEO-*s*-cationic and PEO-*s*-cationic-catechol have the lowest mass detected by QCM-D, which can be assigned to the limitations enforced by electrostatic forces once charge neutralization has been achieved. The adsorbed mass of the PEO-*b*-cationic-catechol block copolymer is clearly larger, which is suggested to be due to the high concentration of catechol groups in the anchoring group that drives adsorption to above the charge neutralization limit. An accumulation of excess positive charges in the adsorbed layer would result in incorporation of small ions and water to neutralize and separate the excess charges, leading to swelling of the layer. Indeed, the relatively high dissipation for this polymer layer suggests that this occurs.

It should be noted that the mass measured by QCM is due to both the adsorbed polymer and that of associated water that oscillates with the crystal. Thus, in all cases, the adsorbed amount is smaller than the mass reported in Table 2, and most significantly so for the most swollen layer, i.e., that formed by the PEO-*b*-cationic-catechol block copolymer.

The two layers formed by polymers with uncharged anchoring blocks (PEO-*b*-catechol and PEO-*s*-catechol) have similar mass, as monitored by QCM and also similar dissipation, suggesting that the adsorbed amount also is similar.

Nanowear and Nanomechanics. We are particularly interested in evaluating how the presence of catechol groups and their distribution in the polymer chain affect the wear resistance of the adsorbed layer. Thus, to this end, we need to also investigate a copolymer without catechol groups, which is the PEO-*s*-cationic copolymer. The wear resistance of the different layers is rather different, and for this reason, we have carried out single scan and multiple scan wear measurements. The results from single scan measurements will be discussed first, followed by data from multiple scan measurements.

Single Scan Measurements. An experiment with an adsorbed layer of the PEO-*s*-cationic polymer is reported in Figure 2. This polymer is anchored to the surface via electrostatic forces, and we find that it is easy to remove a

https://doi.org/10.1021/acs.jpcc.1c06859
J. Phys. Chem. C 2021, 125, 21277−21292

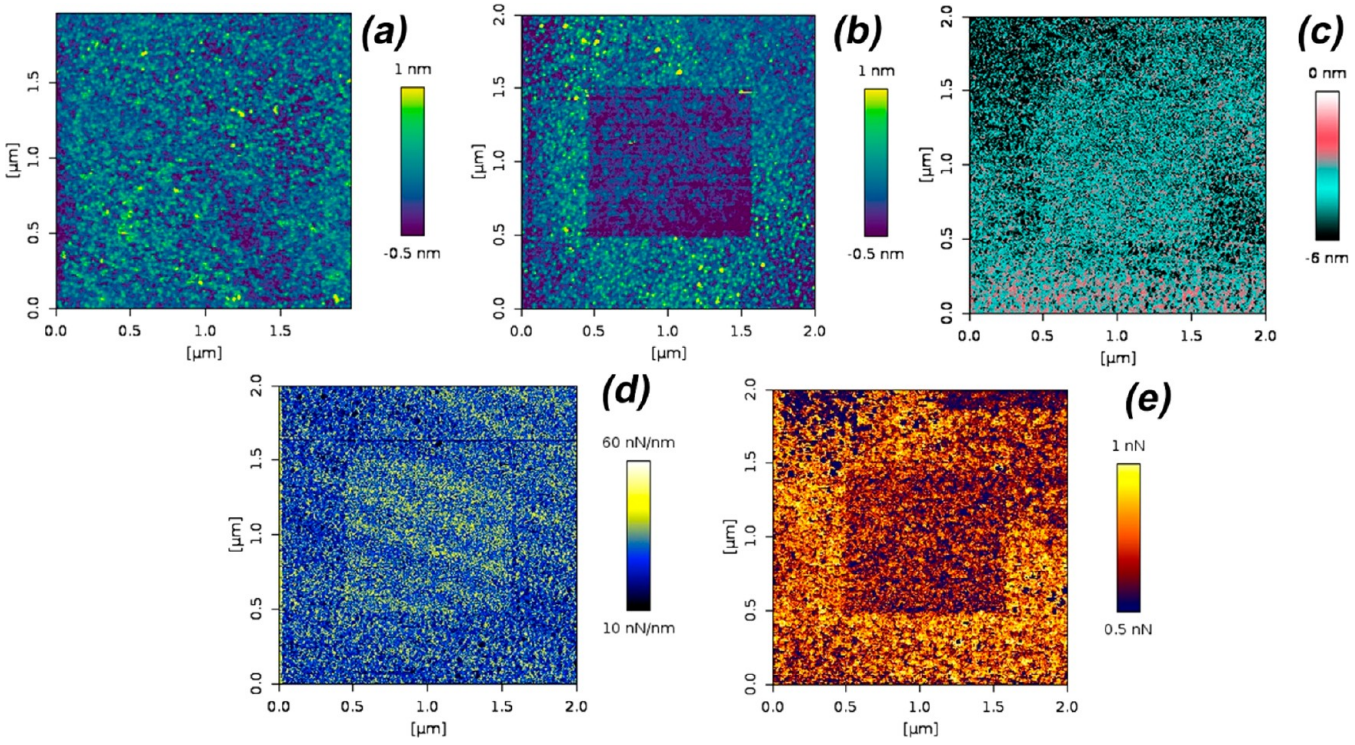

Figure 2. AFM data for the polymer PEO-*s*-cationic adsorbed on silica surfaces. (a) Topography before wear measurements. (b) Topography, (c) deformation, (d) surface stiffness, and (e) adhesion maps recorded after a wear measurement under a load of 75 nN. The worn area is located in the middle part of the images.

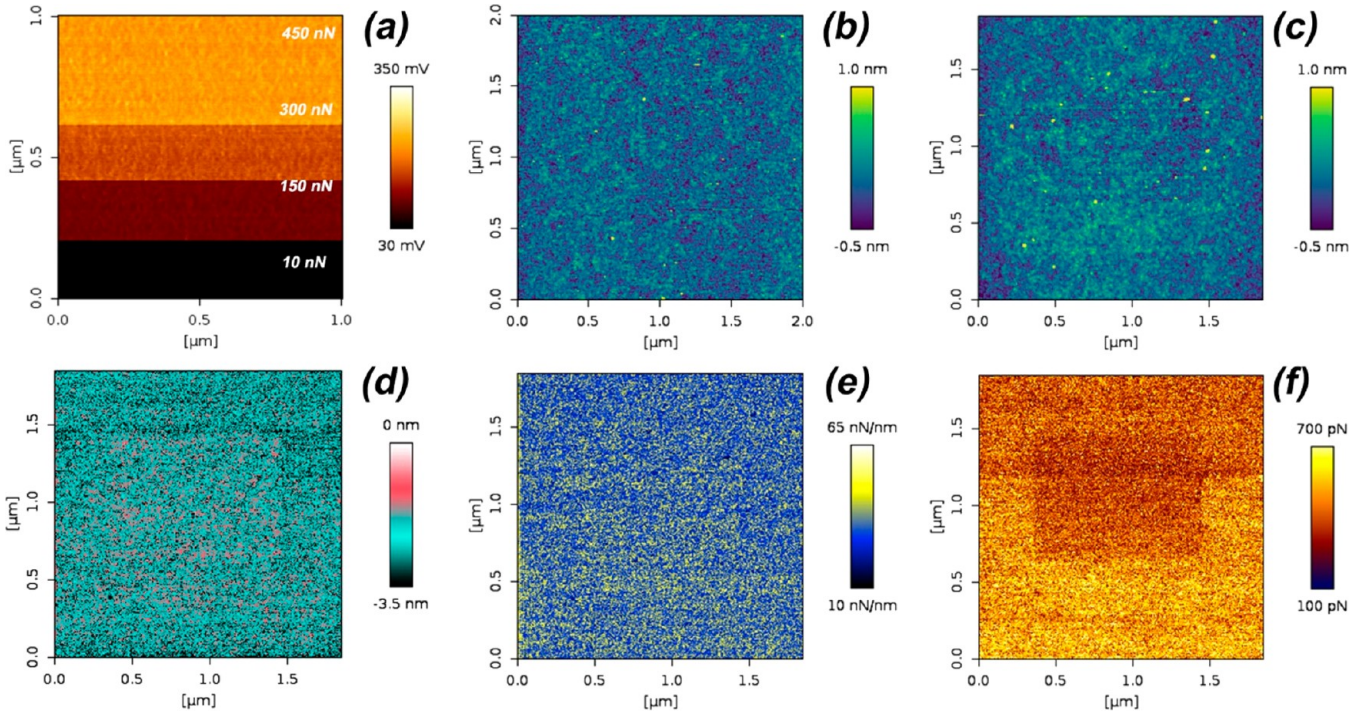

Figure 3. Wear measurements of the adsorbed PEO-*b*-cationic-catechol diblock copolymer on a silica surface. (a) Lateral photodetector response under different loads from bottom to top at 10, 150, 300, and 450 nN. (b) Topography before wear measurements, (c) topography, (d) deformation, (e) surface stiffness, and (f) adhesion after wear measurements under the different loads. The worn area is in the middle of the images. The tip scanned the surface one time.

significant fraction of the layer with only a single path of the tip at a relatively low normal force of 75 nN. The worn area is clearly distinguished in the topography image (Figure 2b), and we also note that the nanomechanical properties are different in the worn area compared to those in the pristine area. The surface deformation is slightly smaller in the worn area than in the pristine area (Figure 2c), which is a direct consequence of the larger surface stiffness in the worn area (Figure 2d). As will be

https://doi.org/10.1021/acs.jpcc.1c06859
J. Phys. Chem. C 2021, 125, 21277−21292

Table 4. Increase in Surface Stiffness, S_{rel}, and Decrease in Magnitude of the Deformation, D_{rel}, in the Worn Area Compared to That of the Undisturbed Layer

polymer	loads				polymer	loads			
PEO-*b*-catechol	150 nN	300 nN	450 nN	300 nN (×3)	PEO-*b*-cationic-catechol	150 nN	300 nN	450 nN	300 nN (×3)
S_{rel} (%)	4.6	4.4	5.6	7.3	S_{rel} (%)	3.7	4.5	6.4	8.5
D_{rel} (%)	17.8	18.5	18.3	25.7	D_{rel} (%)	20.4	21.3	21.7	29.7

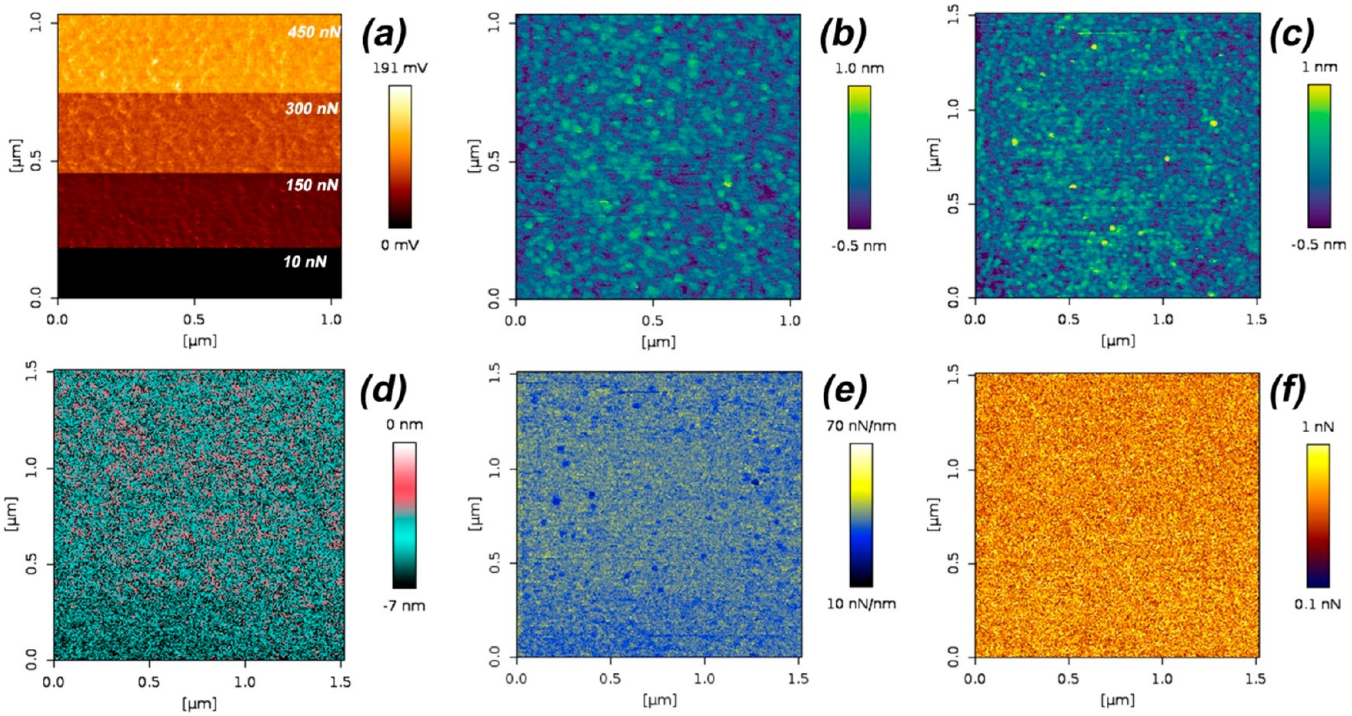

Figure 4. Wear measurements of the adsorbed PEO-*b*-catechol diblock copolymer on a silica surface. (a) Lateral photodetector response under different loads from bottom to top at 10, 150, 300, and 450 nN. (b) Topography before wear measurements, (c) topography, (d) deformation, (e) surface stiffness, and (f) adhesion after wear measurements under the different loads. The worn area is in the middle of the images.

discussed later, the higher stiffness in the worn area is due to the reduced thickness of the layer due to wear. The tip−sample adhesion is also reduced in the worn area (Figure 3e), since there are less polymer molecules per unit area that can bind to the tip. Thus, we can conclude that simultaneous measurements of nanomechanical properties of worn and pristine areas indeed can detect effects due to wear of thin and soft layers on hard surfaces.

We note that the deformation is larger in magnitude than the layer thickness reported in Table 3. When the thickness was calculated as reported in Table 3, the layer was assumed to be homogeneous along the surface and across the layer. Particularly, the second assumption does not reflect the real layer structure with a segment density distribution that decays away from the surface.[52,54,56] Since the deformation is calculated as the difference between the final distance and the distance where the tip first encounters a measurable repulsive force, it means that the longest tails determine the value of the deformation. Thus, a correct interpretation of the data in Figure 2c is that the length of the longest tails is somewhat less after wear, as the polymers can adopt conformations with a larger number of surface contacts as the adsorption density is reduced.

Results from a similar experiment using an adsorbed layer of PEO-*b*-cationic-catechol copolymer on silica are reported in Figure 3. However, as this layer is more wear resistant than that of PEO-*s*-cationic copolymer, we needed to apply a higher normal force to observe any wear. In this case, we used different normal forces in different regions; from bottom to top: 10, 150, 300, and 450 nN. The lateral photodetector signals encountered during the wear measurements are reported in Figure 3a. In this image, it is easy to distinguish the regions where different loads have been applied, which is due to an increased friction force with load. A careful inspection of each load region shows that the photodetector voltage is not constant even when the load is kept the same. Thus, the friction force varies even though the load and sliding speed are constant. This is a sign of stick−slip, and this will be discussed further in a following section. Parts b and c of Figure 3 show the topography before and after the wear measurement, respectively. Clearly, the wear scar for PEO-*b*-cationic-catechol block copolymer is much less obvious even at a load of 450 nN than that obtained for PEO-*s*-cationic polymer at 75 nN. Thus, we conclude that the presence of catechol groups significantly strengthens the binding of the polymer to silica surfaces. Due to the limited wear of the adsorbed PEO-*b*-cationic-catechol block copolymer layer, it is less easy to observe the effect of wear in the nanomechanical images. It is most clearly seen in the adhesion image (Figure 3f), where decreased adhesion is observed at the higher loads. In the deformation (Figure 3d) and stiffness (Figure 3e) images, the worn area is hardly visible, but differences between the worn area at high loads and the pristine surface can be found by evaluating average values and distributions of these values (see Table 4).

https://doi.org/10.1021/acs.jpcc.1c06859
J. Phys. Chem. C 2021, 125, 21277−21292

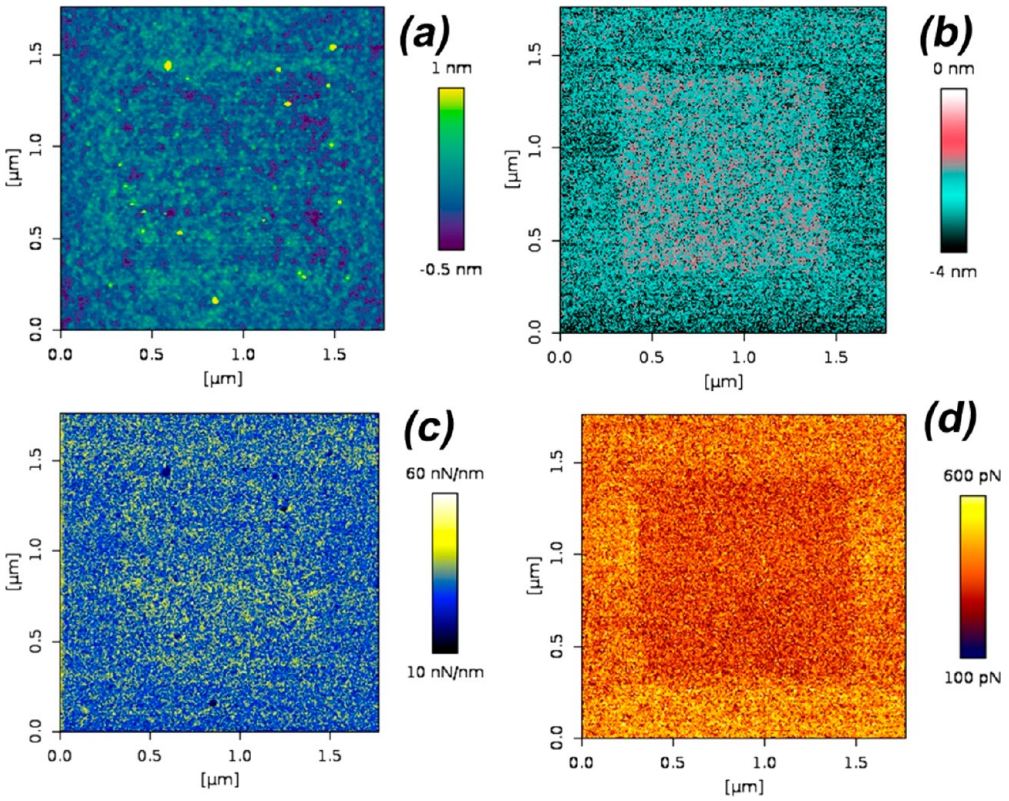

Figure 5. The PEO-*b*-cationic-catechol diblock copolymer adsorbed on silica was worn three times using a force of 300 nN. (a) Topography, (b) deformation, (c) surface stiffness, and (d) adhesion maps after the wear process. The worn area is located in the middle of the images.

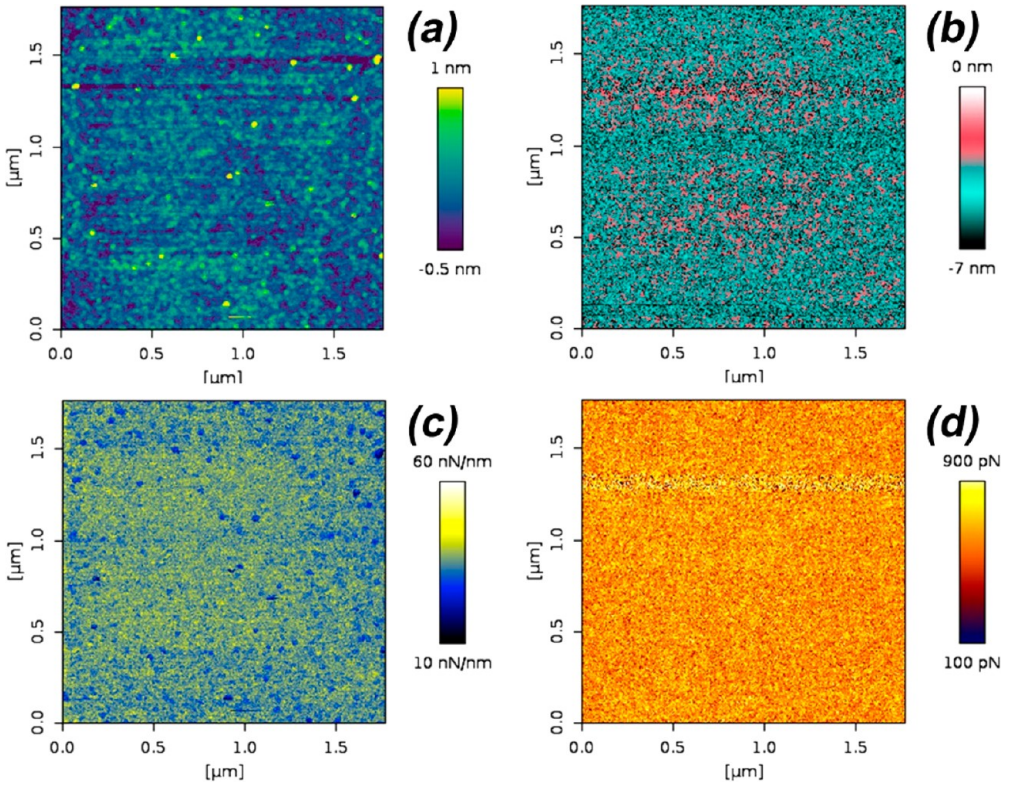

Figure 6. The PEO-*b*-catechol diblock copolymer adsorbed on silica was worn three times using a force of 300 nN. (a) Topography, (b) deformation, (c) surface stiffness, and (d) adhesion maps after the wear process. The worn area is located in the middle of the images.

The same type of experiment for an adsorbed layer of the PEO-*b*-catechol diblock copolymer on silica is shown in Figure 4. In this case also, the lateral photodetector image (Figure 4a) easily distinguishes the different areas that were exposed to

https://doi.org/10.1021/acs.jpcc.1c06859
J. Phys. Chem. C 2021, 125, 21277−21292

different loads. The PEO-*b*-catechol block copolymer does not carry any positive charges, and one could thus expect that it would be less strongly adsorbed to the negatively charged surface than the cationic analogue PEO-*b*-cationic-catechol block copolymer. However, the topography image after wear (Figure 4c) can hardly be distinguished from the topography image recorded before wear (Figure 4b), and the worn area is also difficult to distinguish in the nanomechanical images.

From these measurements, we conclude that adding cationic charges to a diblock copolymer containing a high density of catechol groups does not increase the wear resistance of the layer adsorbed to negatively charged silica surfaces.

Multiple Scan Measurements. To clearly observe wear of our catechol-containing diblock copolymer layers, we need to use more severe conditions than discussed above. The easiest way to do this is to allow the tip to scan the same surface area several times, and results from such measurements will be reported next.

Figure 5 contains data obtained during wear of an adsorbed layer of the PEO-*b*-cationic-catechol diblock copolymer three times using a high load of 300 nN. In the topography image obtained after the wear measurements, one can now distinguish the worn area in the middle of the image (Figure 5a). In particular, one notices that some material has been pushed to the side of the worn area. The effect of the wear is also clearly observed in the deformation image (Figure 5c) where the worn area is less deformed by the tip than the pristine area. Similarly, the tip−sample adhesion is reduced in the worn area (Figure 5d). Less clearly, but nevertheless distinguishable, is that the stiffness is higher in the worn area (Figure 5b). Thus, the same effects of wear on nanomechanical properties are observed during multiple scans at a high load (300 nN) over the PEO-*b*-cationic-catechol block copolymer layer (Figure 5), as observed using a single scan at a low load (75 nN) over the cationic but not catechol-containing PEO-*s*-cationic copolymer (Figure 2).

The same type of experiments was also performed using the uncharged PEO-*b*-catechol diblock copolymer, and the data is reported in Figure 6. In this case, one can also distinguish the worn area in the topography image, including material pushed to the side of the worn area. The deformation is decreased and the stiffness is somewhat increased in the worn area compared to in the surrounding pristine area. On the other hand, and different compared to the cationic analogue, no effect of wear is observed in the adhesion image, suggesting that (close to) the same number of polymer molecules bind to the tip in the worn and unworn area.

The increase in the average stiffness, S, and decrease in magnitude of the average deformation, D, in the worn area relative to the surrounding pristine area, evaluated from the stiffness and deformation images in Figures 3−6, are provided in Table 4. The change in stiffness, S_{rel}, and magnitude of the deformation, D_{rel}, were calculated as

$$S_{rel} = \frac{(S_W - S_p)}{S_p} \tag{3}$$

$$D_{rel} = \left| \frac{(D_W - D_p)}{D_p} \right| \tag{4}$$

where the subscripts w and p stand for the worn and pristine area, respectively.

We note that the stiffness in the worn area increases with load and with repeated scans over the same area. This is due to the decreasing thickness of the soft layer residing on the hard substrate, as supported by the modeling results presented later. Thus, measurements of these nanomechanical properties can be used for a qualitative measure of wear of a soft thin layer on a hard substrate.

Wear Volume. In our previous work,[35] we utilized the relative change in stiffness in the worn and unworn area to qualitatively compare the wear of adsorbed statistical copolymer layers. A more common and quantitative measure of wear is to consider the wear volume. This is challenging when the wear depth is low, as in our case, but possible with the method described in the Methods section. The results of this analysis for the block copolymers used in this work are presented in Figure 7. Since this analysis has not previously been done for the statistical copolymers, we also include data for these in Figure 7.

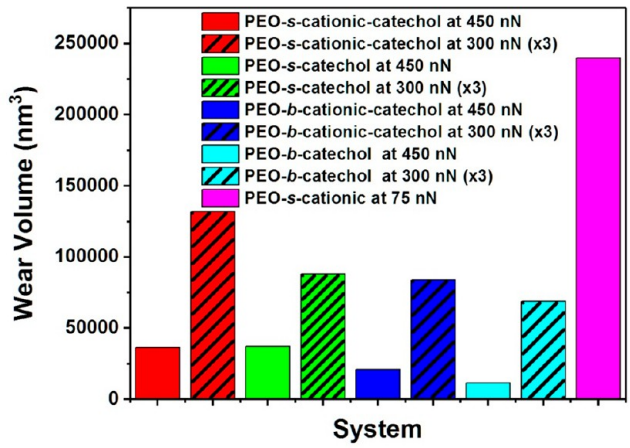

Figure 7. Wear volumes for layers of the studied diblock copolymers. For comparison, we also added data for statistical copolymers studied before[35] but not previously evaluated in terms of wear volume.

The polymer without catechol groups, PEO-*s*-cationic, is significantly more susceptible to wear, and thus, it was exposed only to a low load of 75 nN during a single scan. For the more robust catechol-containing copolymer layers, we present data for a single scan at 450 nN and triple scans at 300 nN. Despite the lower load used, the polymer that does not contain catechol groups clearly has the largest wear volume, which emphasizes the importance of the catechol groups for the wear resistance.

The diblock copolymers, PEO-*b*-catechol and PEO-*b*-cationic-catechol, have higher wear resistance than their counterparts that have a statistical distribution of the two different segments, PEO-*s*-catechol and PEO-*s*-cationic-catechol, signifying that more catechol−surface bonds are formed by the block copolymers. When comparing the wear resistance of the cationic and uncharged version of the catechol-containing polymers, we find that the wear volume is smaller for the uncharged versions both for the diblock copolymers and the statistical polymers. Again, we assign this to the larger amount of catechol−surface bonds for the uncharged copolymers.

Modeling of Layer Stiffness. We found experimentally that the stiffness of the adsorbed layer increased due to wear as a result of its decreased thickness. To elaborate on this, we performed finite element simulations where a stiff tip was pushed toward a thin soft polymer layer. In the simulations, the tip cannot penetrate the layer but only deform it, which is a

https://doi.org/10.1021/acs.jpcc.1c06859
J. Phys. Chem. C 2021, 125, 21277−21292

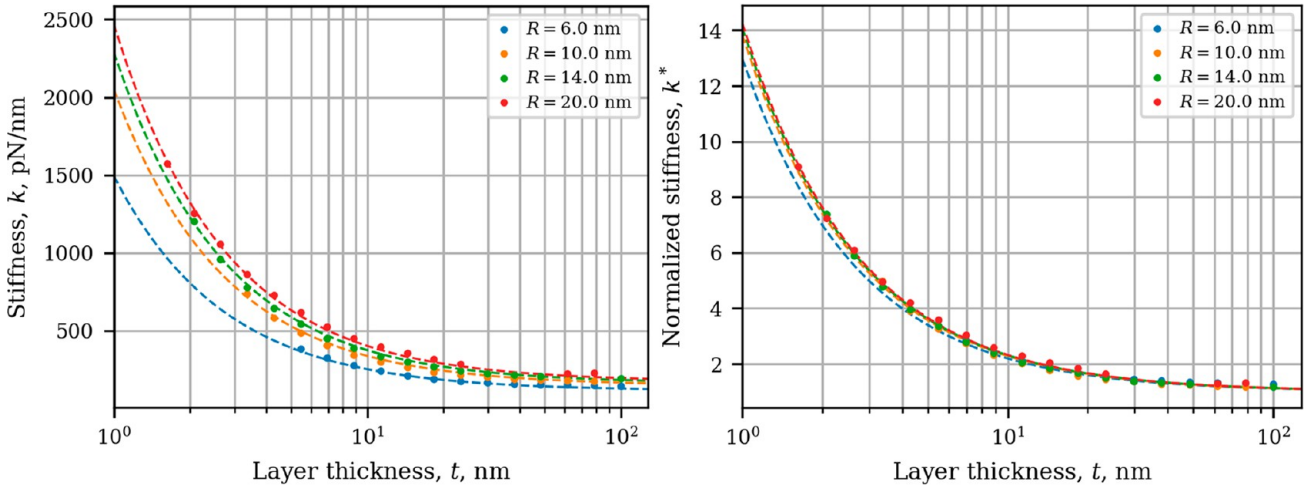

Figure 8. Stiffness as a function of layer thickness for tips with different radii. Data points are results from the simulations, and the dashed lines are from eq 5 fitted to the data with $a = 2688$ pN, $b = -498.2$ pN, $c = -7858$ pN·nm, and $d = 198.2$ pN/nm. (a) As measured stiffness from the simulations and (b) stiffness for a given layer thickness normalized by the stiffness for an infinitely thick layer according to eq 6. Results are obtained from the simulations at a load of 0.5 ± 0.025 nN.

difference compared to the experimental situation where some penetration of the tip into the layer may occur. This approach does not also capture molecular effects such as reduced mobility of polymer chains next to surfaces. Nevertheless, our modeling results demonstrate increasing stiffness with decreasing layer thickness even in this simplified model. The magnitude of the effect is expected to depend on the elastic modulus of the layer and the substrate, but here we focus on the effect of the radius of the tip used for probing the surface, as illustrated in Figure 8.

A simple relationship between the layer thickness, t, and tip radius, R, can be used to describe this effect:

$$k(R, t) = \frac{a}{t} + \frac{b}{R} + \frac{c}{t \cdot R} + d \tag{5}$$

Here a, b, and c are fitting parameters with no obvious physical interpretation and d can be thought of as the stiffness of an infinite thick surface measured with a tip of infinitely large radii. It is of interest to compare the stiffness of a layer with certain thickness to that of an infinitely thick layer with identical properties measured with an identically sized tip. To this end, we calculated the normalized stiffness $k^*(R, t)$ using eq 6

$$k^*(R, t) = \frac{k(R, t)}{k(R, \infty)} \tag{6}$$

The stiffness as a function of the layer thickness determined from the simulated force curves at a load of 0.5 ± 0.025 nN is shown in Figure 8a and illustrates that the measured surface stiffness decreases as the radius of the tip decreases. However, looking at the normalized stiffness in Figure 8b, we see that the effect of the tip radii is small compared to that of the layer thickness. We conclude that there indeed is a foundation for probing wear of soft layers on hard substrates by using local stiffness measurements. The observation that the change in stiffness depends on the probe radius is not an issue when a pristine and worn area is measured simultaneously, as in our case. However, it is an important factor to consider when different surfaces probed by different tips are compared.

Electrostatic vs Catechol Mediated Surface Anchoring. One main finding of this work is that anchoring of the copolymers via catechol mediated interactions provides more robust layers than anchoring via electrostatic forces. Here we have challenged the layers by the combined action of normal forces that compress the layer and lateral forces that may cause the molecules to be displaced along the surface. How readily such a displacement occurs will depend on the lateral interactions between the molecules and the anchoring to the surface. In this paragraph, we consider the mode of surface attachment. It is clear that the higher the energy barrier for moving the polymer from one binding site to another, the less lateral motion will be induced by the probing tip.

The silica surface exposes a high density of silanol groups where some of these acquire a negative charge due to deprotonation in contact with water. It is also clear that the presence of cationic groups next to the surface induces additional deprotonation of the silanol groups.[54,57] Thus, when a cationic polymer moves along the surface, the silanol groups will respond by protonating at the sites where the polymer was initially attached and deprotonating at the new bindings sites. This local surface charge regulation will lower the lateral energy barrier for polymer motion along the surface.

Density functional theory and molecular dynamics simulations have shown that the catechol group adsorbs directly to silica surfaces in water, i.e., without any water between the surface and the catechol group.[33] Through theoretical calculations, it has been estimated that a catechol−silica bond requires a force of 0.5 nN to be broken and the binding energy was estimated to be 23 kcal/mol.[33] The strong binding is due to direct silica−catechol hydrogen bonds, of which 4 can form for each catechol group, as well as dispersion forces. The dispersion forces will be similar along the surface and are not expected to provide any significant lateral energy barrier. In contrast, hydrogen bonds are relatively strong, short-ranged, and highly directional. Even though hydrogen bonds are weak compared to covalent bonds, they are known to form the basis for some of the toughest and strongest materials known such as spider silk,[58] nanocellulose materials,[59,60] and Kevlar.[61] For spider silk, modeling has shown that ordered domains of hydrogen bonds are very difficult to completely break, as they readily reform at new positions.[58] We propose that a similar mechanism explains the high wear resistance of polymers attached to silica via catechol groups.

https://doi.org/10.1021/acs.jpcc.1c06859
J. Phys. Chem. C 2021, 125, 21277−21292

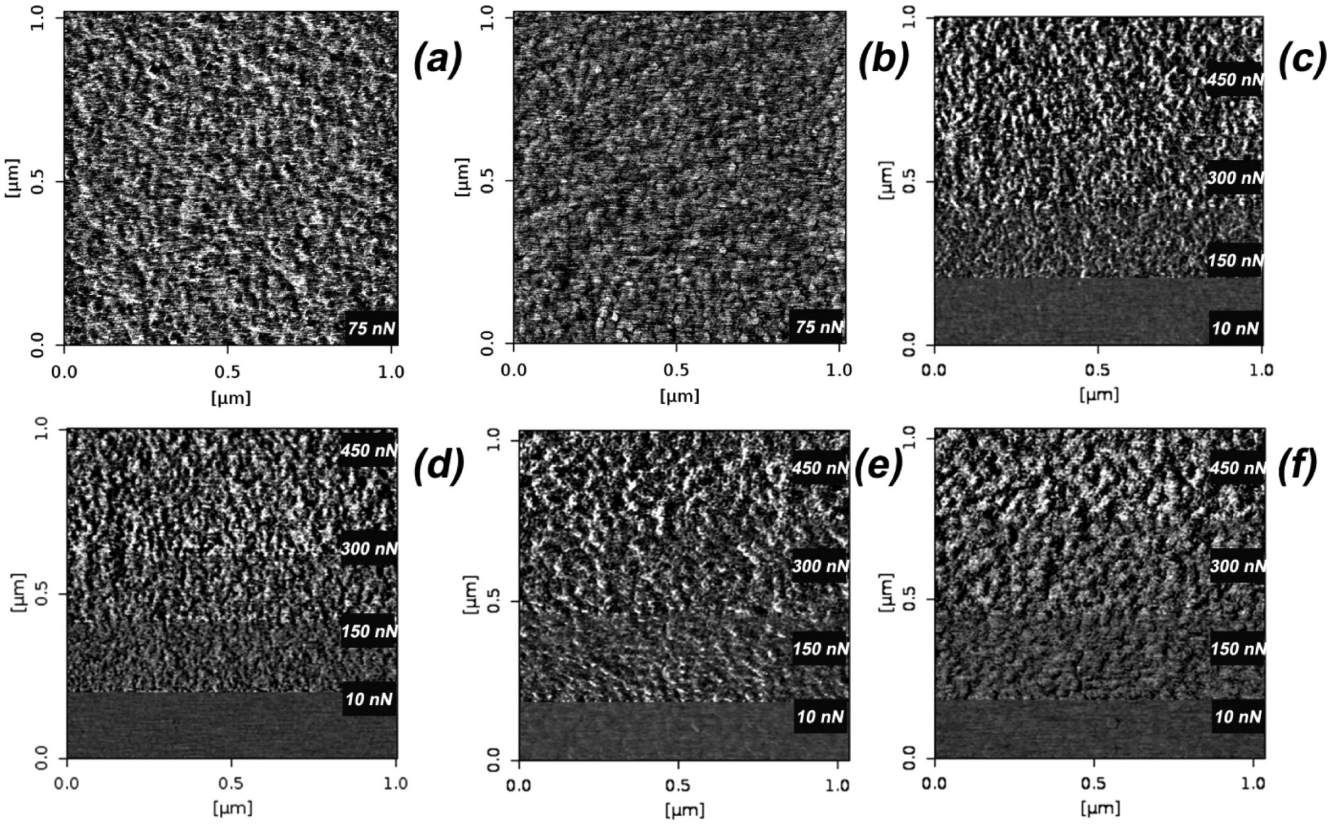

Figure 9. Lateral force images measured during sliding of the AFM tip over a PEO-*s*-cationic copolymer layer on trace (a) and retrace (b) under a load of 75 nN, PEO-*b*-cationic-catechol on trace (c) and retrace (d), and PEO-*b*-catechol on trace (e) and retrace (f) diblock copolymer layers. The applied loads in the different regions in panels c–f are provided in these images. The measurements were done in water.

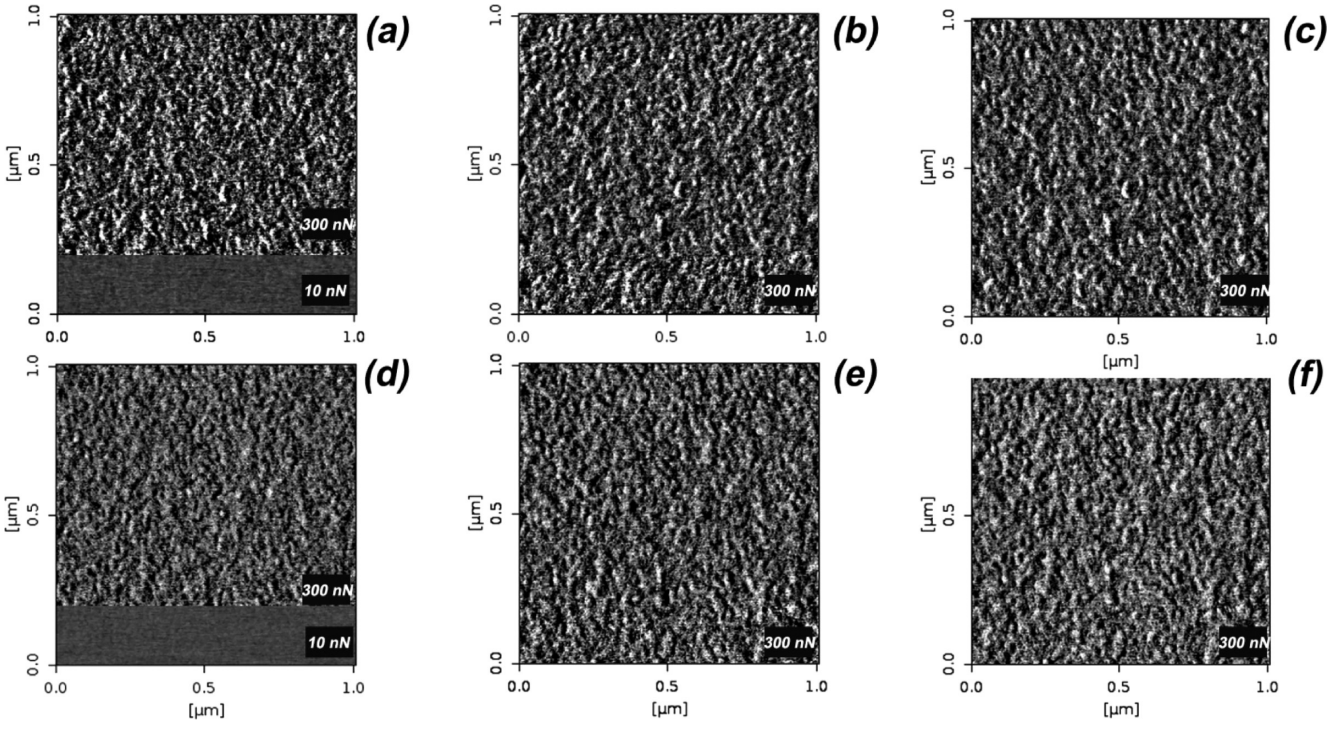

Figure 10. Lateral force images measured during sliding of the AFM tip over a PEO-*b*-cationic-catechol diblock copolymer layer under a load of 300 nN. Data were obtained during trace (a–c) and retrace (d–f) on the first (a, d), second (b, e), and third (c, f) scan over the same area. The measurements were done in water.

https://doi.org/10.1021/acs.jpcc.1c06859
J. Phys. Chem. C 2021, 125, 21277–21292

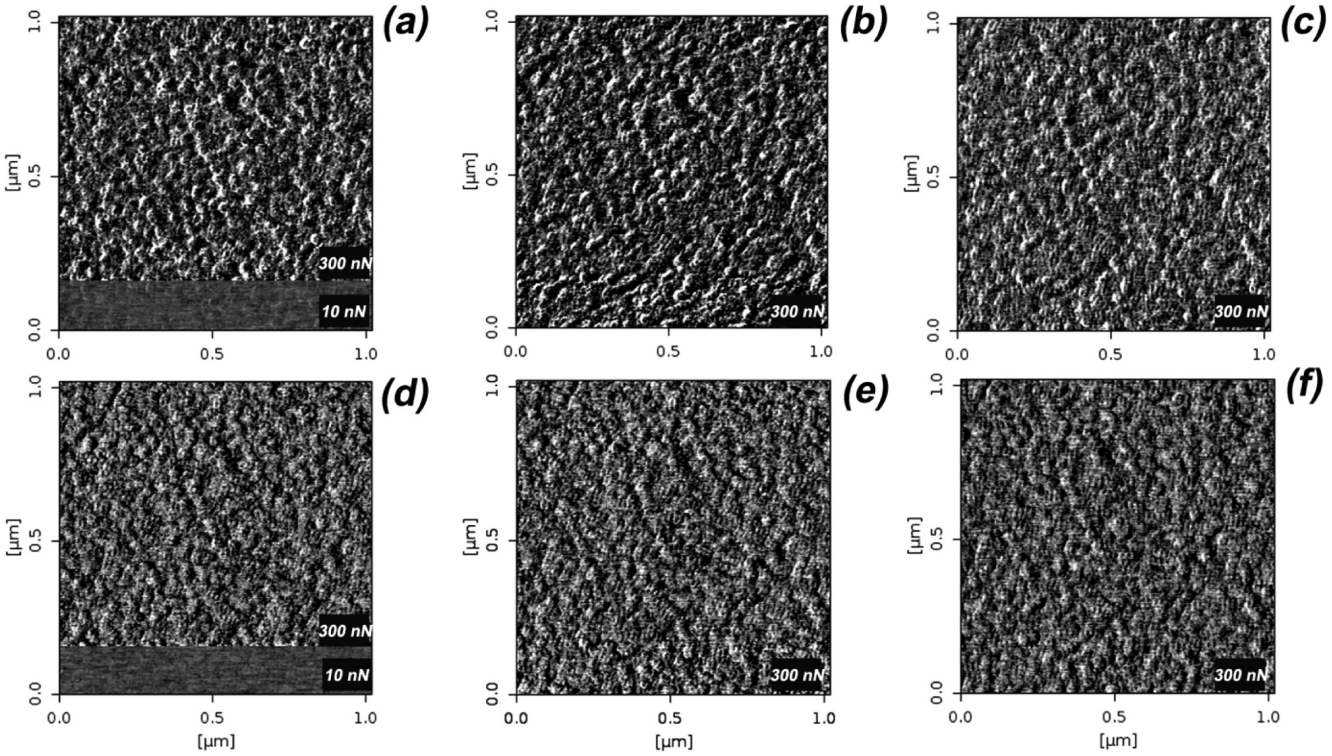

Figure 11. Lateral force images measured during sliding of the AFM tip over a PEO-*b*-catechol diblock copolymer layer under a load of 300 nN. Data were obtained during trace (a−c) and retrace (d−f) on the first (a, d), second (b, e), and third (c, f) scan over the same area. The measurements were done in water.

Statistical vs Diblock Copolymer Adsorption Layers. Diblock copolymer layers have a clear segregation between the adsorbing anchor block that accumulates next to the surface and the buoy block that preferentially resides further away from the surface.[56] In our case, the buoy block contains the 19-unit-long PEO chains, while the anchor block is either non-ionic as in PEO-*b*-catechol or cationic as in PEO-*b*-cationic-catechol. In contrast, the different segments in a statistical copolymer are by necessity less segregated, and one thus would expect a lower number of anchoring segments in contact with the surface for a statistical copolymer compared to that of a similar diblock copolymer.

We have argued that the high wear resistance of the catechol-containing polymers is due to the strong binding of catechol to silica. Thus, it is reasonable to suggest that the more silica−catechol bonds that are formed, the more wear resistance the layer should be. From these arguments, one would expect that the diblock copolymer layers should be more wear resistant than the layers formed by the statistical polymers. The data or the wear volume shown in Figure 7 is consistent with this, but the difference is relatively small.

By considering the change in stiffness and deformation (Table 4) as well as the wear volume during repeated scans (Figure 7), we conclude that the wear resistance of the polymer with an uncharged anchor (PEO-*b*-catechol) block is slightly higher than that for the corresponding copolymers with charged anchor blocks (PEO-*b*-cationic-catechol). Following a similar line of thought as above, we can rationalize this to be partly due to competition for available surface sites between the cationic group and catechol group, leading to somewhat fewer direct catechol−surface bonds when charged groups are present in the anchoring block. It is also partly due to the swelling of the polymer layer due to the excess positive charge in the adsorbed layer, again leading to fewer direct catechol−silica anchoring points. We note that in a previous study[35] using the statistical polymers and single scans a slightly larger wear resistance was found for PEO-*s*-cationic-catechol layers than for PEO-*s*-catechol layers. This conclusion was based on measurements on changes in stiffness and is also observed in the present data at a load of 150 nN (Table 3), but the situation changes at higher loads and during repeated scans (Table 4 and Figure 7) where the PEO-*s*-catechol layers are found to be more wear resistant.

Stick−Slip Features. As briefly noted before, even when the surface layers are challenged by a constant load and at constant sliding speed, there is a variation in the lateral photodetector voltage during sliding due to variations in the friction force. Such variations are typically due to stick−slip phenomena. In some cases, the stick−slip occurs irregularly, e.g., due to surface roughness effects, and in other cases, it occurs with a characteristic stick−slip length (i.e., with a characteristic distance between two stick events), as typically observed for polymers that deform plastically during the combined action of load and shear.[38,39] To analyze this situation, one utilizes the lateral photodetector images recorded during wear. Data obtained at different loads for adsorbed layers formed by the polymers PEO-*s*-cationic copolymer, PEO-*b*-cationic-catechol, and PEO-*b*-catechol are shown in Figure 9. Similar data are shown in Figures 10 and 11 for the two diblock copolymers, as they are worn three times over the same area at a load of 300 nN.

Qualitatively, one notices that the images reported in Figure 9 have different features at different loads, where the features tend to become larger at larger loads. This is a sign of a larger stick−slip length at higher loads. To analyze this quantitatively requires a 2D FFT of the images as reported in detail in our previous work.[35,39]

https://doi.org/10.1021/acs.jpcc.1c06859
J. Phys. Chem. C 2021, 125, 21277−21292

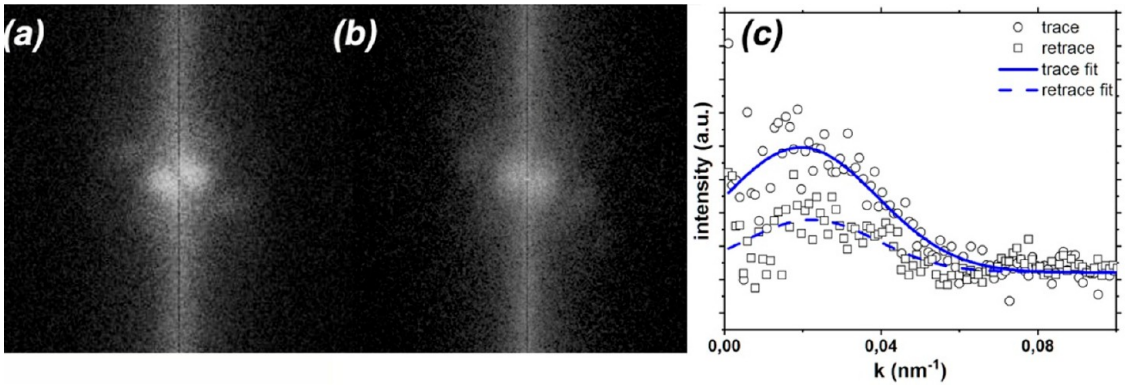

Figure 12. Two-dimensional FFT images of the lateral force variation measured during sliding of the AFM tip over a silica surface with an adsorbed layer of PEO-*s*-cationic copolymer on trace (a) and retrace (b) at a load of 75 nN. The images were constructed from the data reported in Figure 9a,b. The degree of correlation decreases from bright to dark. Panel c illustrates the corresponding 1D FFT plot evaluated from the 2D images. The Gaussian fitting curves are shown as solid and dashed lines for trace and retrace, respectively.

The load dependence of the stick−slip will not be discussed further in this article, but we will instead pay attention to if the stick−slip pattern is affected by first sliding the tip in one direction (trace) and back along the same line in the other direction (retrace), and if it is affected by scanning the same area several times. To this end, we will present FFT analyses of the images reported in Figure 9a,b for the PEO-*s*-cationic copolymer layer at 75 nN and in Figures 10 and 11 for the PEO-*b*-cationic-catechol and PEO-*b*-catechol block copolymer layers under a load of 300 nN.

Following the procedure described in the Methods section, 2D FFT spectra of the images reported in Figure 9a,b were obtained and these are shown in Figure 12a,b. The radial integration converts these images into 1D spectra in *k*-space (Figure 12c). In this plot, we can distinguish one peak located at $k \approx 0.02$ nm^{-1}, which corresponds to a characteristic stick−slip length of about 50 nm in both the trace and retrace images. However, the peak is more pronounced in the trace image. This suggests that the initial sliding (trace) along the surface under a load of 75 nN changes the layer structure. In addition to the wear observed (Figure 2), it is plausible to suggest flattening of the layer and bending of the adsorbed polymers in the sliding direction. If these structural changes do not recover during the time scale of one trace−retrace cycle (1 s), they will affect the stick−slip pattern. From the data in Figure 12, we draw the conclusion that wear, flattening, and bending of the adsorbed polymer layer may all reduce the intensity of the stick−slip pattern but hardly affect the peak position, i.e., the characteristic stick−slip length.

The 2D FFT spectra obtained for the block copolymer layers are shown in Figure 13. In these images, it is possible to distinguish a partial outer ring, particularly clearly seen for the uncharged PEO-*b*-catechol polymer layer. This suggests the presence of two characteristic stick−slip lengths for the catechol-containing polymer layers. Indeed, the 1D FFT functions reported in Figure 14 display two peaks. The presence of two peaks is not due to the diblock structure, as two peaks also have been observed for statistical copolymers containing catechol groups. For the statistical copolymers, the peaks at smaller distances (larger *k*-values) were more pronounced for the uncharged version of the copolymer,[35] as also observed for the diblock copolymers in this study. Thus, the presence of the small stick−slip length (below 20 nm, Figure 15) is assigned to result from the strong binding of catechol groups to the surface. As the

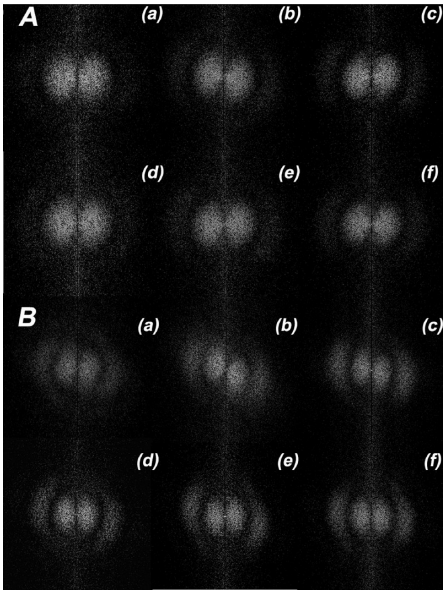

Figure 13. Two-dimensional FFT images of the lateral force variation measured during sliding of the AFM tip over a silica surface with an adsorbed layer of PEO-*b*-cationic-catechol on trace (panel A, a−c) and retrace (d−f) evaluated from the region exposed to 300 nN normal load repeated three times and reported in Figure 10. The corresponding data for silica with an adsorbed layer of PEO-*b*-catechol on trace (panel B, a−c) and retrace (d−f) evaluated from the region exposed to 300 nN normal load three times and reported in Figure 11. The degree of correlation decreases from bright to dark. Data obtained during the first, second, and third scans are shown in images a and d, b and e, and c and f, respectively.

adsorbed polymer binds to the tip, it becomes stretched and the tip will slip when the tip−polymer attachment is broken. The longer stick−slip length is on the other hand associated with dragging the tip along the atomically rough silica surface (RMS roughness ≈ 0.2−0.3 nm), which also may result in dragging of some polymers along the surface and thus wear. Indeed, a similar stick−slip length has been reported for the bare silica surface, which suggests that the underlying silica surface structure is of key importance.[35] As for the PEO-*s*-cationic copolymer layer, we observe similar stick−slip lengths on trace and retrace.

For the catechol-containing diblock copolymers, we find no clear difference in magnitude of the peak observed at low *k*-

https://doi.org/10.1021/acs.jpcc.1c06859
J. Phys. Chem. C 2021, 125, 21277−21292

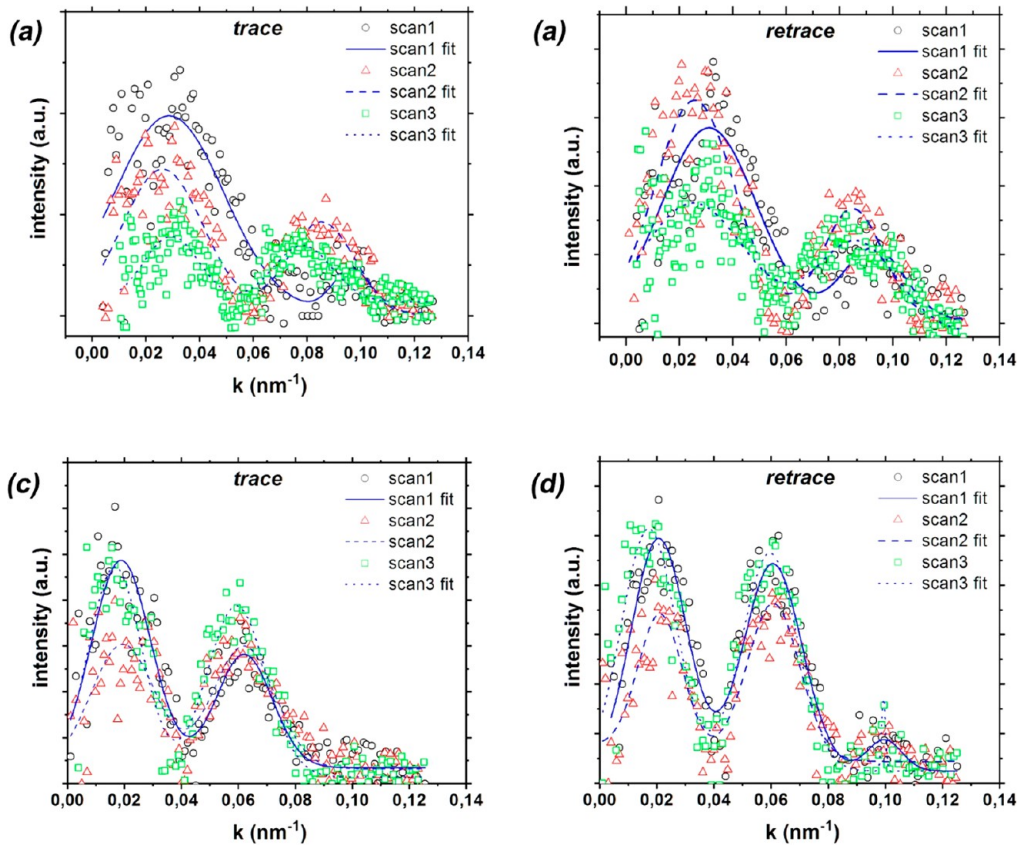

Figure 14. One-dimensional FFT plot of the lateral force variation evaluated from the 2D images shown in Figure 13. The data are for an adsorbed layer of PEO-*b*-cationic-catechol on trace (a) and retrace (b) and for an adsorbed layer of PEO-*b*-catechol on trace (c) and retrace (d) at a load of 300 nN. The Gaussian fittings are shown as solid curves for the first scan, dashed curves for the second scan, and dotted curves the third scan.

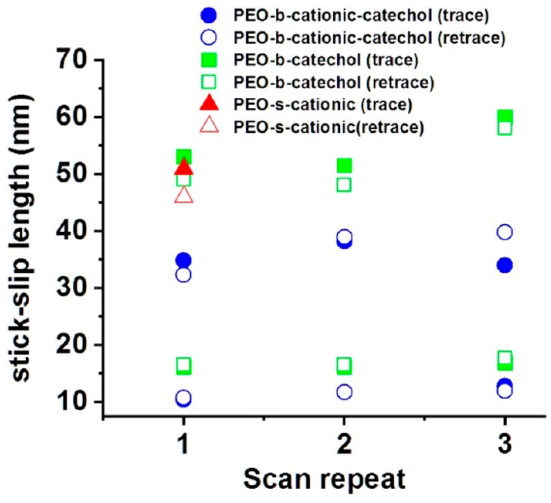

Figure 15. Characteristic stick−slip length for the catechol-containing diblock copolymer layers as a function of repeated scans at 300 nN evaluated from the peak position in the 1D FFT correlation function shown in Figures 12 and 14. For comparison, the stick−slip length for layers of the PEO-*s*-cationic copolymer evaluated at 75 nN is also shown.

values in the 1D FFT obtained from the lateral photodetector signal during trace and retrace, which is in contrast to what was observed for the PEO-*s*-cationic copolymer layer. All of these layers are expected to flatten and polymers to bend in the direction of the moving tip as the layers are challenged by load and shear, but the data for the catechol-containing diblock copolymers suggest that this is not very important. Instead, the main difference between on one hand the PEO-*s*-cationic copolymer layer and on the other hand the catechol-containing diblock copolymer layers is the higher wear of the former. Thus, we assign the difference in peak amplitude found for the PEO-*s*-cationic copolymer layer during trace and retrace to be due to mainly wear. Some wear also explains why the amplitude of the peak found at small *k*-values tends to shift downward with the number of scans for the PEO-*b*-cationic-catechol polymer layer, whereas this trend is less clear for the even more wear resistant PEO-*b*-catechol polymer layer.

The second peaks found at high *k*-values (Figure 14) are slightly stronger on retrace than on trace for the catechol-containing diblock copolymers, suggesting that additional catechol−surface bonds are formed when the layer is challenged by load and shear. Thus, the anchoring to the surface becomes stronger during the wear measurements, which further enhances the wear resistance. It seems plausible that similar effects play a role for mussel adhesive proteins, where enhancement of the binding strength could be expected when the mussel binding site is challenged by predators, waves, and currents.

The effect of repeated wear measurements on the stick−slip lengths is small, as seen in Figure 15. Thus, the peak position in the 1D FFT curves is hardly affected by the limited wear. On the other hand, the peak amplitude is more clearly affected by wear, as discussed above.

https://doi.org/10.1021/acs.jpcc.1c06859
J. Phys. Chem. C 2021, 125, 21277−21292

CONCLUSIONS

Our measurements of wear and nanomechanical properties with nanometer resolution have shown that indeed adsorbed layers of catechol-containing polymers on silica surfaces are significantly less subject to wear in water than similar polymers anchored by electrostatic forces alone. This is largely due to the strong direct hydrogen bonding between catechol and silica that allows displacement of water from the silica surface. Our data show that the uncharged catechol block provides a stronger anchoring to the negatively charged silica surface than the block containing both cationic charges and catechol groups. Based on QCM-D data, we suggest that this is due to the formation of a more compact adsorbed layer, allowing more catechol groups to bind, when the anchoring block is uncharged. In contrast, a high concentration of excess cationic charges at the silica surface is unfavorable and leads to swelling of the layer and less catechol−surface anchoring points. The diblock copolymers show higher wear resistance than their statistical counterparts, which we again assign to the larger number of catechol−silica contacts in the diblock copolymer layers.

Partial wear of the polymer layers changes the nanomechanical properties of the layer. The tip−sample adhesion is reduced by wear as less polymers bind to the probing AFM tip. At the same time, the stiffness of the soft layer on the hard surface increases as the layer becomes thinner. This feature was reproduced by a simple elastic contact mechanics model. The deformation under a given load was also reduced as the layer was becoming thinner by wear.

The sliding of the AFM tip over the adsorbed layer was characterized by stick−slip motion. For the polymer layer without catechol groups, one characteristic stick−slip length was observed. The value of the stick−slip length was similar during trace and retrace, but the peak intensity was reduced on retrace, which is assigned to wear. In contrast, the sliding of the AFM tip above the catechol diblock copolymer layers was characterized by two distinct stick−slip lengths. The longer of these, with a similar value as that for the catechol-free polymer, was assigned to be due to moving the polymer along the surface, while the shorter one that was unique for the catechol-containing diblock copolymers was assigned to stretching of firmly anchored polymers. In this case also, wear reduces the amplitude of the long distance stick−slip peak assigned to dragging the polymer along the surface. Interestingly, the short distance peak assigned to stretching the polymer was slightly larger on retrace than trace, which suggests that more catechol−surface bonds are formed as a result of the combined action of load and shear.

ASSOCIATED CONTENT

Supporting Information

The Supporting Information is available free of charge at https://pubs.acs.org/doi/10.1021/acs.jpcc.1c06859.

Synthesis and characterization of the diblock copolymers, examples of QCM-D primary data, and illustration of the modeling experiment (PDF)

AUTHOR INFORMATION

Corresponding Authors

Illia Dobryden − *Experimental Physics, Division of Materials Science, Department of Engineering Sciences and Mathematics, Luleå University of Technology, Luleå SE-971 87, Sweden;* orcid.org/0000-0001-6877-9282; Email: illia.dobryden@ltu.se

Per Martin Claesson − *KTH Royal Institute of Technology, School of Engineering Sciences in Chemistry, Biotechnology and Health, Department of Chemistry, Division of Surface and Corrosion Science, SE-100 44 Stockholm, Sweden;* Email: percl@kth.se

Authors

Medeina Steponavičiūtė − *Institute of Chemistry, Vilnius University, LT-03225 Vilnius, Lithuania*

Daniel Hedman − *Applied Physics, Division of Materials Science, Department of Engineering Sciences and Mathematics, Luleå University of Technology, Luleå SE-971 87, Sweden; Center for Multidimensional Carbon Materials, Institute for Basic Science (IBS), Ulsan 44919, Republic of Korea*

Vaidas Klimkevičius − *Institute of Chemistry, Vilnius University, LT-03225 Vilnius, Lithuania*

Ričardas Makuška − *Institute of Chemistry, Vilnius University, LT-03225 Vilnius, Lithuania*

Andra Dėdinaitė − *KTH Royal Institute of Technology, School of Engineering Sciences in Chemistry, Biotechnology and Health, Engineering Pedagogics, SE-100 44 Stockholm, Sweden; RISE Research Institutes of Sweden, Division of Bioscience and Materials, SE-114 86 Stockholm, Sweden*

Xiaoyan Liu − *School of Chemistry and Chemical Engineering, Shaanxi Normal University, Xi'an 710062, China;* orcid.org/0000-0001-5503-015X

Robert W. Corkery − *KTH Royal Institute of Technology, School of Engineering Sciences in Chemistry, Biotechnology and Health, Department of Chemistry, Division of Surface and Corrosion Science, SE-100 44 Stockholm, Sweden;* orcid.org/0000-0002-7461-2232

Complete contact information is available at: https://pubs.acs.org/10.1021/acs.jpcc.1c06859

Notes

The authors declare no competing financial interest.

ACKNOWLEDGMENTS

X.L. acknowledges financial support from the National Natural Science Foundation of China (NSFC) (21902098).

REFERENCES

(1) Waite, J. H. Evidence for a Repeating 3,4-dihydroxyphenylalanine- and Hydroxyproline- Containing Decapeptide in the Adhesion Protein of the Mussel, Mytilus Edulic L. *J. Biol. Chem.* **1983**, *258*, 2911−2915.

(2) Waite, J. H.; Housley, T. J.; Tanzer, M. L. Peptide Repeats in a Mussel Glue Protein: Theme and Variations. *Biochemistry* **1985**, *24*, 5010−5014.

(3) Waite, J. H. Adhesion a la Moule. *Integr. Comp. Biol.* **2002**, *42*, 1172−1180.

(4) Lee, H.; Lee, K. D.; Pyo, K. B.; Park, S. Y.; Lee, H. Catechol-Grafted Poly(ethylene glycol) for PEGylation on Versatile Substrates. *Langmuir* **2010**, *26*, 3790−3793.

(5) White, J. D.; Wilker, J. J. Underwater Bonding with Charged Polymer Mimics of Marine Mussel Adhesive Proteins. *Macromolecules* **2011**, *44*, 5085−5088.

(6) Matos-Pérez, C. R.; Wilker, J. L. Ambivalent Adhesives: Combining Biomimetic Cross-Linking with Antiadhesive Oligo-(ethylene glycol). *Macromolecules* **2012**, *45*, 6634−6639.

(7) Patil, N.; Falentin-Daudré, C.; Jérome, C.; Detrembleur, C. Mussel-Inspired Protein-Repelling Ambivalent Block Copolymers: Controlled Synthesis and Characterization. *Polym. Chem.* **2015**, *6*, 2919−2933.

(8) North, M. A.; Del Grosso, C. A.; Wilker, J. J. High Strength Underwater Bonding with Polymer Mimics of Mussel Adhesive Proteins. *ACS Appl. Mater. Interfaces* **2017**, *9*, 7866−7872.
(9) Horsch, J.; Wilke, P.; Pretzler, M.; Seuss, M.; Melnyk, I.; Remmler, D.; Fery, A.; Rompel, A.; Börner, H. G. Polymerizing Like Mussels Do: Toward Synthetic Mussel Foot Proteins and Resistant Glues. *Angew. Chem., Int. Ed.* **2018**, *57*, 15728−15732.
(10) Steponaviciute, M.; Klimkevicius, V.; Makuska, R. Synthesis and Properties of Cationic Gradient Brush Copolymers Carrying PEO Side Chains and Catechol Moieties. *Macromol. Chem. Phys.* **2021**, *222*, 2000364.
(11) Steponaviciute, M.; Klimkevicius, V.; Makuska, R. Synthesis and Stability against Oxidation of Random Brush Copolymers Carrying PEO Side Chains and Catechol Moieties. *Mater. Today Commun.* **2020**, *25*, 101262.
(12) Lee, B. P.; Messersmith, P. B.; Israelachvili, J. N.; Waite, J. H. Mussel-Inspired Adhesives and Coatings. *Annu. Rev. Mater. Res.* **2011**, *41*, 99−132.
(13) Ye, Q.; Zhou, F.; Liu, W. Bioinspired Catecholic Chemistry for Surface Modification. *Chem. Soc. Rev.* **2011**, *40*, 4244−4258.
(14) Sedo, J.; Saiz-Poseu, J.; Busgué, F.; Ruiz-Molina, D. Catechol-Based Biomimetic Functional Materials. *Adv. Mater.* **2013**, *25*, 653−701.
(15) Moulay, S. Dopa/Catechol-Tethered Polymers: Bioadhesives and Biomimetic Adhesive Materials. *Polym. Rev.* **2014**, *54*, 436−513.
(16) Ma, S.; Wu, Y.; Zhou, F. Bioinspired Synthetic Wet Adhesives: from Permanent Bonding to Reversible Regulation. *Curr. Opin. Colloid Interface Sci.* **2020**, *47*, 84−98.
(17) Kord Forooshani, P.; Lee, B. P. Recent Approaches in Designing Bioadhesive Materials Inspired by Mussel Adhesive Protein. *J. Polym. Sci., Part A: Polym. Chem.* **2017**, *55*, 9−33.
(18) Razaviamri, S.; Wang, K.; Liu, B.; Lee, B. P. Catechol-Based Antimicrobial Polymers. *Molecules* **2021**, *26*, 559.
(19) Silverman, H. G.; Roberto, F. F. Understanding Marine Mussel Adhesion. *Mar. Biotechnol.* **2007**, *9*, 661−681.
(20) McBride, M. B.; Wesselink, L. G. Chemisorption of Catechol on Gibbsite, Boehmite, and Noncrystalline Alumina Surfaces. *Environ. Sci. Technol.* **1988**, *22*, 703−708.
(21) Taylor, S. W.; Luther, G. W., III; Waite, J. H. Polarographic and Spetrophotometric Investigation of Iron(III) Complexation to 3,4-dihydroxyphenylalanine-Containing Peptides and Proteins from Mytilus Edulis. *Inorg. Chem.* **1994**, *33*, 5819−5824.
(22) Zhang, F.; Pan, J.; Claesson, P. M.; Brinck, T. Electrochemical, Atomic Force Microscopy and Infrared Reflection Absorption Spectroscopy Studies of Pre-Formed Mussel Adhesive Films on Carbon Steel for Corrosion Protection. *Thin Solid Films* **2012**, *520*, 7136−7143.
(23) Zhang, F.; Brinck, T.; Brandner, B. D.; Claesson, P. M.; Dedinaite, A.; Pan, J. In-situ Confocal Raman Micro-Spectroscopy and Electrochemical Studies of Mussel Adhesive Protein and Ceria Composite Film on Carbon Steel in Salt Solutions. *Electrochim. Acta* **2013**, *107*, 276−291.
(24) Zhang, F.; Sababi, M.; Brinck, T.; Persson, D.; Claesson, P. M.; Pan, J. In Situ Investigations of Fe^{3+} Induced Complexation of Adsorbed Mefp-1 Protein Films on Iron Substrate. *J. Colloid Interface Sci.* **2013**, *404*, 62−71.
(25) Anderson, T. H.; Yu, J.; Estrada, A.; Hammer, M. U.; Waite, J. H.; Israelachvili, J. N. The Contribution of DOPA to Substrate-Peptide Adhesion and Internal Cohesion of Mussel-Inspired Synthetic Peptide Films. *Adv. Funct. Mater.* **2010**, *20*, 4196−4205.
(26) Lee, B. P.; Chao, C.-Y.; Nunalee, F. N.; Motan, E.; Shull, K. R.; Messersmith, P. B. Rapid Gel Formation and Adhesion in Photocurable and Biodegradable Block Copolymers with High DOPA Content. *Macromolecules* **2006**, *39*, 1740−1748.
(27) Lu, Q.; Danner, E.; Waite, J. H.; Israelachvili, J. N.; Zeng, H.; Hwang, D. S. Adhesion of Mussel Foot Proteins to Different Substrate Surfaces. *J. R. Soc., Interface* **2013**, *10*, 20120759.
(28) Krivosheeva, O.; Dedinaite, A.; Claesson, P. M. Adsorption of Mefp-1: Influence of pH on Adsorption Kinetics and Adsorbed Amount. *J. Colloid Interface Sci.* **2012**, *379*, 107−113.
(29) Levine, Z. A.; Rapp, M. V.; Wei, W.; Mullen, R. G.; Wu, C.; Zerse, G. H.; Mittal, J.; Waite, J. H.; Israelachvili, J. N.; Shea, J.-E. Surface Force Measurements and Simulations of Mussel-Derived Peptide Adhesives on Wet Organic Surfaces. *Proc. Natl. Acad. Sci. U. S. A.* **2016**, *113*, 4332−4337.
(30) Leng, C.; Liu, Y.; Jenkins, C.; Meredith, H.; Wilker, J. J.; Chen, Z. Interfacial Structure of DOPA-Inspired Adhesive Polymer Studied by Sum Frequency Generation Vibrational Spectroscopy. *Langmuir* **2013**, *29*, 6659−6664.
(31) Mian, S. A.; Saha, L. C.; Jang, J.; Wang, L.; Gao, X.; Nagase, S. Density Functional Theory Study of Catechol Adhesion on Silica Surfaces. *J. Phys. Chem. C* **2010**, *114*, 20793−20800.
(32) Mian, S. A.; Gao, X.; Nagase, S.; Jang, J. Adsorption of Catechol on a Wet Silica Surface: Density Functional Theory Study. *Theor. Chem. Acc.* **2011**, *130*, 333−339.
(33) Mian, S. A.; Yang, L.-M.; Saha, L. C.; Ahmed, E.; Ajmal, M.; Ganz, E. A Fundamental Understanding of Catechol and Water Adsorption on a Hydrophilic Silica Surface: Exploring the Underwater Adhesion Mechanism of Mussels on an Atomic Scale. *Langmuir* **2014**, *30*, 6906−6914.
(34) Mian, S. A.; Khan, Y. The Adhesion Mechanism of Marine Mussel Foot Protein: Adsorption of L-Dopa on α- and β- Cristobalite Silica using Density Functional Theory. *J. Chem.* **2017**, *2017*, 8756519.
(35) Dobryden, I.; Steponaviciute, M.; Klimkevicius, V.; Makuska, R.; Dedinaite, A.; Liu, X.; Corkery, R. W.; Claesson, P. M. Bioinspired Adhesion Polymers: Wear Resistance of Adsorption Layers. *Langmuir* **2019**, *35*, 15515−15525.
(36) Colaço, R. From Nano and Microcontacts to Wear of Materials. In *Fundamentals of Friction and Wear at the Nanosclae*; Gnecco, E., Meyer, E., Eds.; Springer International Publishing: Heidelberg, 2015.
(37) Colaço, R.; Serra, A. P. Nanoscale Wear of Hard Materials: An Overview. *Curr. Opin. Colloid Interface Sci.* **2020**, *47*, 118−125.
(38) D'Acunto, M.; Dinelli, F.; Pinque, P. Nanowear of Polymers. In *Fundamentals of Friction and Wear at the Nanoscale*; Gnecco, E., Meyer, E., Eds.; Springer International Publishing: Heidelberg, 2015; pp 545−587.
(39) He, Y.; Dobryden, I.; Pan, J.; Ahniyaz, A.; Deltin, T.; Corkery, R. W.; Claesson, P. M. Nano-Scale Mechanical and Wear Properties of a Waterborn Hydroxyacrylic-Melamine Anti-Corrosion Coating. *Appl. Surf. Sci.* **2018**, *457*, 548−558.
(40) He, Y.; Li, G.; Hwang, K.-H.; Boluk, Y.; Claesson, P. M. Nano-Scale Mechanical and Wear Properties of a Corrosion Protective Coating Reinforced by Cellulose Nanocrystals - Initiation of Coating Degradation. *Appl. Surf. Sci.* **2021**, *537*, 147789.
(41) Claesson, P. M.; Dobryden, I.; Li, G.; He, Y.; Huang, H.; Thorén, P.-A.; Haviland, D. From Force Curves to Surface Nanomechanical Properties. *Phys. Chem. Chem. Phys.* **2017**, *19*, 23642−23657.
(42) Dobryden, I.; Yang, Z.; Claesson, P. M.; Pileni, M. P. Water Dispersive Suprastructures: An Organizational Impact on Nano-mechanical Properties. *Adv. Mater. Interfaces* **2021**, *8*, 2001687.
(43) Nicolas-Boluda, A.; Yang, Z.; Dobryden, I.; Carn, F.; Winckelmans, N.; Péchoux, C.; Bonville, P.; Bals, S.; Claesson, P. M.; Gazeau, F.; Pileni, M. P. Intracellular Fate of Hydrophobic Nanocrystal Self-Assemblies in Tumor Cells. *Adv. Funct. Mater.* **2020**, *30*, 2004274.
(44) Alvarez-Asencio, R.; Thormann, E.; Rutland, M. W. Determination of Torsional Spring Constant of Atomic Force Microscopy Cantilevers: Combining Normal Spring Constant and Classical Beam Theory. *Rev. Sci. Instrum.* **2013**, *84*, No. 096102.
(45) Quignon, B.; Pilkington, G. A.; Thormann, E.; Claesson, P. M.; Ashfold, M. N. R.; Mattia, D.; Leese, H.; Davis, S. A.; Briscoe, W. H. Sustained Frictional Instabilities of Nanodomed Surfaces: Stick-Slip Amplitude Coefficient. *ACS Nano* **2013**, *7*, 10850−10862.
(46) Wojas, N. A.; Dobryden, I.; Wallqvist, V.; Swerin, A.; Järn, M.; Schoelkopf, J.; Gane, P. A. C.; Claesson, P. M. Nanoscale Wear and Mechanical Properties of Calcite: Effects of Stearic Acid Modification and Water Vapor. *Langmuir* **2021**, *37*, 9826−9837.

https://doi.org/10.1021/acs.jpcc.1c06859
J. Phys. Chem. C 2021, 125, 21277−21292

(47) Ishak, M. I.; Jenkins, J.; Kulkarni, S.; Keller, T. F.; Briscoe, W. H.; Nobbs, A. H.; Su, B. Insights into Complex Nanopillar-Bacteria Interactions: Roles of Nanotopography and Bacterial Surface Proteins. *J. Colloid Interface Sci.* **2021**, *604*, 91−103.
(48) Sauerbrey, G. Verwendung von Schwingquarzen zur Wägung dünner Schichten und zur Mikrowägung. *Eur. Phys. J. A* **1959**, *155*, 206−222.
(49) Rivlin, R. Large Elastic Deformations of Isotropic Materials. I. Fundamental Concepts. *Philos. Trans. R. Soc., A* **1997**, 23−54.
(50) Rivlin, R. S. Large Elastic Deformation of Isotropic Materials. II. Some Uniqueness Theorems of Pure, Homogeneous Deformation. *Philos. Trans. R. Soc., A* **1948**, *240*, 491−508.
(51) Rivlin, R. Large Elastic Deformations of Isotropic Materials. III. Some Simple Problems in Cylindrical Polar Co-ordinates. *Philos. Trans. R. Soc., A* **1948**, *240*, 509−525.
(52) Linse, P. Adsorption of Weakly Charged Polyelectrolytes at Oppositely Charged Surfaces. *Macromolecules* **1996**, *29*, 326−336.
(53) Linse, P.; Claesson, P. M. Modeling of Bottle-Brush Polymer Adsorption onto Mica and Silica Surfaces. *Macromolecules* **2009**, *42*, 6310−6318.
(54) Shovsky, A.; Knohl, S.; Dedinaite, A.; Zhu, K.; Kjøniksen, A.-L.; Nyström, B.; Linse, P.; Claesson, P. M. Cationic Poly(N-isopropylacrylamide) Block Copolymer Adsorption Investigated by Dual Polarization Interferometry and Lattice Mean-Field Theory. *Langmuir* **2012**, *28*, 14028−14038.
(55) Van de Steeg, H. G. M.; Cohen Stuart, M. A.; de Keizer, A.; Bijsterbosch, B. H. Polyelectrolyte Adsorption: A Subtle Balance of Forces. *Langmuir* **1992**, *8*, 2538−2546.
(56) Evers, O. A.; Scheutjens, J. M. H. M.; Fleer, G. J. Statistical Thermodynamics of Block Copolymer Adsorption. *J. Chem. Soc., Faraday Trans.* **1990**, *86*, 1333−1340.
(57) Wolterink, J. K.; Koopal, L. K.; Cohen Stuart, M. A.; van Riemsdijk, W. H. Surface Charge Regulation upon Polyelectrolyte Adsorption, Hematite, Polystyrene Sulfonate, Surface Charge Regulation. Theoretical Calculations and Hematite-Poly(Styrene Sulfonate) System. *Colloids Surf., A* **2006**, *291*, 13−23.
(58) Keten, S.; Xu, Z.; Ihle, B.; Buehler, M. J. Nanoconfinement Controls Stiffness, Strength and Mechanical Toughness of β-sheet Crystals in Silk. *Nat. Mater.* **2010**, *9*, 359−367.
(59) Hishikawa, Y.; Togawa, E.; Kondo, T. Characterization of Individual Hydrogen Bonds in Crystalline Regenerated Cellulose using Resolved Polarized FTIR Spectra. *ACS Omega* **2017**, *2*, 1469−1476.
(60) Tayeb, A. H.; Amini, E.; Ghasemi, S.; Tajvidi, M. Cellulose Nanomaterials - Binding Properties and Applications: A Review. *Molecules* **2018**, *23*, 2684.
(61) Roenbeck, M. R.; Sandoz-Rosado, E. J.; Cline, J.; Wu, V.; Moy, P.; Afshari, M.; Reichert, D.; Lustig, S. R.; Strawhecker, K. E. Probing the Internal Structures of Kevlar Fibers and their Impacts on Mechanical Performance. *Polymer* **2017**, *128*, 200−210.

https://doi.org/10.1021/acs.jpcc.1c06859
J. Phys. Chem. C 2021, 125, 21277−21292